Modelling of chemical and magnetic order in Ni-Mn-Al shape memory alloys using Monte Carlo simulations.

Alejandro Alés[1,2,*] and Fernando Lanzini[1,2]

[1] *Instituto de Física de Materiales Tandil (IFIMAT), Universidad Nacional del Centro de la Provincia de Buenos Aires (UNCPBA), Pinto 399, 7000 Tandil, Argentina*
[2] *Consejo Nacional de Investigaciones Científicas y Técnicas (CONICET), Godoy Cruz 2290 (C1425FQB) CABA, Argentina*
[*] *aales@ifimat.exa.unicen.edu.ar*

Abstract

A model for the description of atomic and magnetic ordering in $Ni-Mn-Al$ shape memory alloys is presented. The energetic parameters for the chemical and magnetic interactions are estimated from fitting to experimental data. Monte Carlo simulations based on this model correctly reproduce the critical $B2 \leftrightarrow L2_1$ ordering temperatures as a function of composition for three pseudobinary composition lines, as well as the nature of the low temperature magnetic transition. A ferromagnetic configuration is predicted for alloys in the stable $L2_1$ structure, whereas an antiferromagnetic state is obtained for metastably retained $B2$ order; this is in agreement with experimental observations. It is found that atomic ordering is mainly governed by $Ni-Al$ interactions, and that the formation of $B2$ order can delay stabilization at low temperatures of the $L2_1$ configuration; the magnetic type of ordering depends on the $Mn-Mn$ distance.

1 Introduction

Ternary $Ni-Mn-Al$ alloys, as other $Ni-Mn$ based alloys, display interesting shape memory and magnetic properties. Shape memory properties are connected with a martensitic transformation that takes place from a high temperature ordered *bcc* (austenite) structure to a low temperature phase (martensite) with a complex stacking sequence. This transformation is diffusionless and related to several phenomena (pseudoelasticity, shape memory effect, etc) with technological applications. The range of compositions of interest is around Ni_2MnAl, although the martensitic transformation occurs for off-stoichiometric compounds [1–3]. The magnetic properties are determined by the atomic configuration (order) in the austenite phase: at the temperatures of interest, this can be either $B2$ (*bcc* with order in nearest neighbours) or $L2_1$ (*bcc* ordered in nearest and next-nearest neighbours). If the atomic distribution is $B2$, the alloy magnetically orders to an antiferromagnetic (afm) state, whereas if the atomic order is $L2_1$, it results in a ferromagnetic (fm) configuration [1, 4].

The type and degree of atomic ordering depend, in turn, on temperature and composition, being the $B2$ configuration stable at high temperatures and transforming to $L2_1$ upon cooling. Kainuma et al.[1] determined the critical temperatures for the $L2_1 \rightarrow B2$ transition for alloys with different compositions around stoichiometric Ni_2MnAl. In all the range of interest ($c_{Ni} \simeq 50-57at.\%$, $c_{Al} \simeq 20-30at.\%$, $c_{Mn} \simeq 18-25at.\%$), the measured $T_{L2_1 \rightarrow B2}$ was between $\simeq 730-800K$. It has been shown that the thermal treatment directly influences the temperature of the magnetic transition and the martensitic transformation [5]. For instance, the M_s temperature of martensitic transformation diminishes as the alloy is aged below the ordering temperature; this has been explained as due to the stabilization of the parent phase on ordering [6, 7]. Despite long term annealing below the ordering temperature, an homogeneous $L2_1$ phase cannot be obtained, since a fraction of the $B2$ phase remains present [2] [8]. Then a mixed $fm-L2_1$ and $afm-B2$ state occurs, with close-lying Curie and Néel temperatures [3]. As has been proposed, the combination of films with different magnetic phases (fm-afm or afm-pm) can produce negative magnetorresistance effect [9].

With regards to the magnetic properties, Ziebeck and Webster [10] measured by means of X-rays and neutron diffraction the stoichiometric alloy Ni_2MnAl. After quenching, a $B2$ superlattice was detected: the magnetic configuration was defined as an antiferromagnetic cone spiral, where the collinear components are coupled ferromagnetically in (1 1 1) sheets with antiferromagnetic coupling between adjacent planes. Morito et al. [4] obtained the Néel temperatures (T_N) for alloys with fixed 50 at. $\%Ni$ and order $B2$ retained by quenching. These T_N´s are $\approx 290-300K$ and almost independent of composition. They also found that, in some compositions, the appearance of the $L2_1$ phase suppress the martensitic transformation. This result highlights the relevance of atomic ordering in connection with potential shape memory applications. Acet et al. [2] studied the magnetic properties of stoichiometric Ni_2MnAl in $B2$ and $L2_1$ phases by means of X-ray diffraction, magnetization, magnetic susceptibility and specific heat measurements, and found evidence of the ferromagnetic character of the $L2_1$ phase. They concluded that the magnetic coupling is essentially governed by the $Mn-Mn$ distance: at larger distances (as in the $L2_1$ configuration) the coupling is ferromagnetic, and at smaller distances it tends to be antiferromagnetic. These authors found also that the $B2$ phase can be readily retained as a metastable state at room temperature, and that the devel-

opment of the thermodynamically more favorable $L2_1$ phase is hindered by kinetics.

Several works have applied first-principles calculations to study the magnetic properties of the austenitic phase: Enkovaara et al. [11] studied $L2_1 - Ni_2MnAl$ using both LDA and GGA methods, finding the magnetization planes, determining that the magnetic moments are localized in manganese atoms and estimating the Curie temperature. The line of compositions $Ni_2Mn_xAl_{2-x}$ $(0 < x < 2)$ was studied by Büsguen et al. [12], using GGA method with ultrasoft pseudopotentials and allowing tetragonal distortion to the structures. It has been found that, depending on manganese concentration, the most stable configuration could be ferromagnetic or antiferromagnetic. For low x the Mn atoms place mutually as third neighbours, and the leading interaction is of the ferromagnetic type, whereas for Mn contents higher than around 28 at.% ($x \approx 1.125$) the ground state is antiferromagnetic. Yang et al. [13] studied the full-Heusler $L2_1$ phase in Ni_2MnAl and showed the relevance of the magnetic moments on stabilizing this structure against tetragonal distortions. Galanakis and Şaşıoğlu [14] employed a full-potential ab-initio approach and studied a simple model to estimate the magnetic exchange energies for the $B2$ and $L2_1$ structures. These authors confirmed that the distance among Mn atoms determine the particular type of ground state magnetic structure (ferro- or antiferromagnetic). Simon et al. [15] studied the magnetic properties of stoichiometric Ni_2MnAl with different degrees of long-range chemical order by ab-initio methods, using the single-site coherent potential approximation (CPA) to study the disordered cases. Besides, these authors study the evolution of magnetism at finite temperatures using Monte Carlo simulations, assuming that the atomic configuration remains fixed.

As can be seen from the list above, most theoretical studies in this alloy system have been restricted to the stoichiometric Ni_2MnAl alloy, and thermal effects are usually disregarded. The aim of the present work is the development of a relatively simple model that allows accounting for off-stoichiometric effects, thermal disorder, and that includes the interplay between the atomic and magnetic degrees of freedom. To this end, we implemented a model based on Monte Carlo (MC) simulations that accounts for simultaneous evolution of the type and degree of atomic and magnetic order. A Blume-Emery-Griffiths Hamiltonian is employed to describe the energetics of the atomic configuration and an Ising model is used to account for the magnetic degrees of freedom. The chemical energetic parameters were determined by fitting to the experimentally reported atomic ordering temperatures and the exchange energy for magnetic interactions were obtained by the mean field theory, considering that the magnetic moments are localized in the manganese atoms [16]. The model is able to reproduce the experimentally observed nature of atomic and magnetic phases ($B2-$, $L2_1-$, $-pm$, $-fm$, $-afm$) and the transition temperatures.

The outline of the work is presented as follows: in section 2 the MC implementation is described and the relevant order parameters are defined. In section 3 the results are presented: first, a set of energetic interactions that allows reproduction of different experimental observations are proposed, three pseudobinary lines of the phase diagram are calculated and the thermal evolution of the ordering is discussed. Conclusions are summarized in section 4.

2 Methodology

Monte Carlo simulations of the atomic ordering were performed in the canonical ensemble. The crystal was simulated in a virtual *bcc* cell with periodic boundary conditions. To every site i of the lattice, two pseudo-spin variables are assigned: σ_i, which describes the atomic species, and S_i, describing the magnetic state. The variable σ_i takes any of the three values $+1, 0, -1$, corresponding to Ni, Mn, and Al atoms, respectively. The variable S_i can take the values $+1, 0, -1$ and are associated to magnetic moment pointing upwards, no magnetic moment, or magnetic moment pointing downwards, respectively. The non-zero magnetic moments have been assigned to Mn atoms ($S_i = \pm 1$), whereas Ni and Al do not contribute to magnetism ($S_i = 0$). Atomic (magnetic) ordering proceeded by direct interchange of nearest neighbours atoms (spin fliping) using the Metropolis criterion [17], as detailed in [18].

The overall Hamiltonian is expressed as the sum of magnetic and chemical (or configurational) terms $\mathcal{H} = \mathcal{H}_{chem} + \mathcal{H}_{magn}$.

The chemical energy of the system is obtained by a Blume-Emery-Griffiths Hamiltonian [19] extended up to second neighbours [20, 21]

$$\mathcal{H}_{chem} = \mathcal{H}^{(1)}_{chem} + \mathcal{H}^{(2)}_{chem}$$

where

$$\mathcal{H}^{(k)}_{chem} = J_k(\sum_{<ij>} \sigma_i\sigma_j) + K_k(\sum_{<ij>} \sigma_i^2\sigma_j^2) + L_k(\sum_{<ij>} (\sigma_i^2\sigma_j + \sigma_i\sigma_j^2)) \tag{1}$$

here $k = 1, 2$ refers to the coordination sphere, such that $\mathcal{H}^{(1)}_{chem}$is the nearest neighbours contribution, and the second term $\mathcal{H}^{(2)}_{chem}$ the contribution of next-nearest neighbour pairs. The parameters J_k, K_k and L_k are linear combinations of the interchange energies $W^{(k)}_{AB}$:

$$J_k = \frac{W^{(k)}_{NiAl}}{4}$$

$$K_k = \frac{2W^{(k)}_{NiMn} + 2W^{(k)}_{MnAl} - W^{(k)}_{NiAl}}{4}$$

$$L_k = \frac{W^{(k)}_{NiMn} - W^{(k)}_{MnAl}}{4}$$

These interchange energies are defined in terms of the interaction potential $V^{(k)}_{AB}$ as $W^{(k)}_{AB} = -2V^{(k)}_{AB} + V^{(k)}_{AA} + V^{(k)}_{BB}$ and are the key quantities to define the ordering tendency between the different atomic species that constitute the alloy. For $W^{(k)}_{AB} > 0$ there is an ordering tendency for $A - B$ pairs placed as k-th neighbours, whereas $W^{(k)}_{AB} < 0$ indicates tendency to clustering [22, 23].

The magnetic Hamiltonian is represented by the Ising model

$$\mathcal{H}_{magn} = \sum_{s} \sum_{\langle ij \rangle} J_m^s S_i S_j$$

where J_m^s is the magnetic coupling between the magnetic atoms placed as s-th neighbours. If all the interaction energies are negative, they lead to the ferromagnetic order. In the case of energies that are not all negative, the magnetic ordering depends on the ratio between the energies as a function of the coordination sphere [24, 25].

One of the aims of the present work is the determination of a set of energetic parameters (the chemical interchange energies $W_{AB}^{(k)}$ and the magnetic coupling constants J_s^M). The first quantities were determined by means of successive approximations to the available experimental data concerning chemical order-disorder temperatures. Besides, the magnetic exchange energies were calculated employing mean field theory. Whereas the chemical interactions are assumed to be restricted to first and second neighbours, a suitable description of the magnetic phenomena required the inclusion of up to third neighbours interactions.

To quantify the degree of atomic order, the general *bcc* lattice is subdivided into four interpenetrating *fcc* sublattices, labeled $I - IV$ in Figure 1. Long range ordering (*lro*) structures are defined by means of the probabilities p_A^k of an atom of type A occupying the $k-th$ sublattice. For instance, in the long range disordered configuration ($A2$) it is $p_A^k = c_A, \forall k$. In the $B2$ state there is ordering in nearest neighbours (*nn*), and $p_A^I = p_A^{II} \neq p_A^{III} = p_A^{IV}$. The $L2_1$ configuration is ordered in first and second neighbours (*nnn*): $p_A^I = p_A^{II} \neq p_A^{III} \neq p_A^{IV}$. These probabilities are not all independent, and a simpler description can be done through the following six independent parameters [20, 23]:

$$x_A = \frac{p_A^I + p_A^{II} - p_A^{III} - p_A^{IV}}{4}$$

$$y_A = \frac{p_A^I - p_A^{II}}{2}$$

$$z_A = \frac{p_A^{III} - p_A^{IV}}{2}$$

with A any two of the atomic species. The parameter x_A measures ordering in *nn* ($x_A = 0$ in $A2$ phase, $x_A \neq 0$ for $B2$ or $L2_1$), whereas z_A (or y_A) is a measure of the ordering in *nnn*: $z_A = 0$ for $A2$ and $B2$, $z_A \neq 0$ in the $L2_1$ phase.

Although above the order–disorder transition temperature the long range order disappears, some correlation in the occupation of nearby sites could persist. This short range order (*sro*) is disregarded in mean field approaches such as the Bragg-Williams-Gorski (BWG) method, and treated in an approximated way in higher approximations of the cluster variation method [26]. One advantage of MC simulations is that it treats the *sro* correlations, in principle, exactly. In order to quantify the degree of *sro*, we have counted the total number of atomic pairs for first, second and third neighbors and then divided by the total number of atoms.

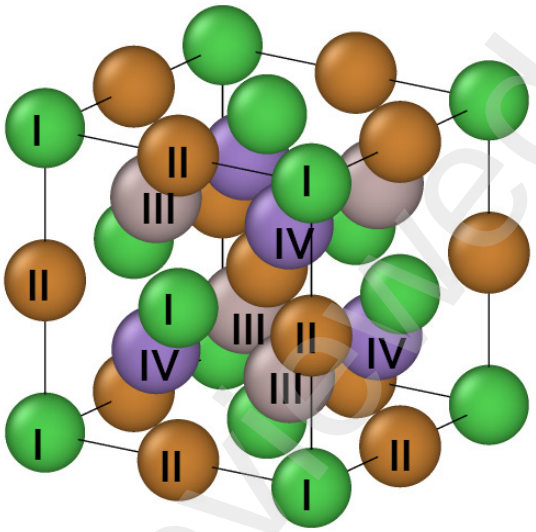

Figure 1: Four interpenetrating *fcc* sublattices that form a *bcc*-type structure.

Since we will deal with alloys with magnetic properties, magnetization will be defined by means of the global parameter $m = p_\uparrow - p_\downarrow$, or the sublattice magnetizations $m = p_\uparrow^k - p_\downarrow^k$, with $k = I, ..., IV$, being $p_{\uparrow(\downarrow)}^k$ the probability of a magnetic moment being oriented upwards or downwards, respectively.

3 Results

3.1 Determination of atomic interchange energies, ordering temperatures

Simulations of heating runs with a temperature step $\Delta T = 10K$ were performed on lattices containing $2 \cdot 32^3$ sites. For the evaluation of the energy and subsequent proposal of exchange of positions, the sites had been chosen at random; when the number of proposal is equal to lattice size, a MC step is made. In order to reach thermal equilibrium, 500000 MC steps were performed at each temperature.

The initial state was chosen as an $L2_1$ configuration with the maximum degree of order compatible with the composition. The numerical values for the six chemical interchange energies $W_{AB}^{(k)}$, have been determined by fitting to the experimental order-disorder temperatures reported by Kainuma et al. [1]. These authors measured the critical ordering temperatures $T_{L2_1 \rightarrow B2}$ for compositions around stoichiometric Ni_2AlMn, and grouped them into three lines for a better description: line A corresponds to fixed $50at.\%Ni$, line B to fixed $25at.\%Mn$, and line C to $25at.\%Al$, with $c_{Ni} \geq 50\%$ in all the cases.

The interchange energies have been determined by a method of successive approximations, taking as starting point the mean field (Bragg-Williams-Gorski, BWG) estimates obtained in [1].

It is known [22, 27, 28] that the interchange energies obtained by fitting to experimental order-disorder tempera-

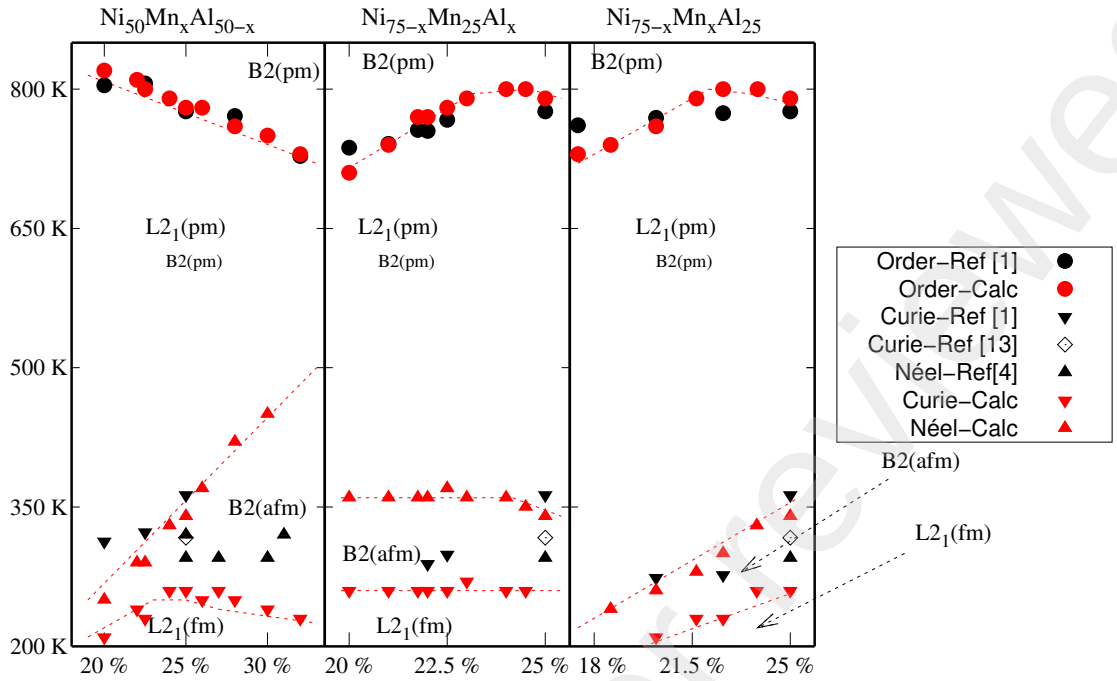

Figure 2: Experimental and calculated critical temperatures of ordering $T_{L2_1 \to B2}$, Curie temperature T_C when $L2_1$ is present and Neel temperature T_N when the alloy has $B2$ structure.

Pair	$W_{AB}^{(1)}$	$W_{AB}^{(2)}$
Ni-Al	3130 (2600)	620 (465)
Ni-Mn	745 (600)	70 (0)
Al-Mn	1250 (1014)	575 (519)

Table 1: Set of chemical energies obtained in this work. For comparison, in parentheses are the BWG values [1].

tures using the BWG analytical expressions are underestimations of the values that will reproduce the same critical temperatures within higher hierarchies in the Cluster Variation Method [26]. In fact, when using the BWG values from [1] for the present system within the MC simulations, the predicted critical temperatures were lower than the experimental values.

Thus, a readjustment of the interchange energies was performed, varying their values until a satisfactory agreement with the experimental $T_{L2_1 \to B2}$ was achieved. The converged values are listed in table 1. These values are about 20% higher than the values proposed by [1]. The dominant contribution for the ordering arise from the $Ni - Al$ pairs interaction in first-neighbours, which have a strong ordering tendency. Similar results were obtained in other ternary alloy systems, such as $Cu-Al-Ni$ [29–32] where the strongest contribution to order stems from first neighbours $Ni - Al$ pairs.

In Fig. 2 the calculated order-disorder temperatures are compared with the experimental results [1] for the three different composition lines. A general good agreement with the experimental data is obtained, with the critical temperatures being in the range between 700 and $800K$. For the line with 50% at. Ni (left panel in Fig. 2), a decrease of $T_{B2 \leftrightarrow L2_1}$ with the Mn content is predicted, in agreement with the experimental results. For the line with fixed 25% at. Mn, $T_{B2 \leftrightarrow L2_1}$ is correctly predicted to increase with the Al content, but there is a decrease near the composition Ni_2MnAl. This effect is, also, observable in the line with fixed 25% at. Al, where the higher transition temperature ocurrs near 22% at. Mn. The interaction of the second neighbors $Ni - Al$ is slightly higher than $Al - Mn$ in the same coordination sphere, which could explain this phenomenon.

Moreover, we have performed simulations up to a temperature of 1600 K and the $B2 \to A2$ transition has not been observed. This fact coincides with what was observed experimentally, where the alloys show $B2$ order up to the melting temperature [1].

In Fig. 3 the thermal evolution of the *lro* and *sro* parameters for stoichiometric Ni_2MnAl is shown. The parameter $|x_{Mn}|$ is non-zero and almost constant ($\simeq 0.25$) in all the range of studied temperatures (red line); this shows that the Mn atoms remains located, mostly, in sublattices III/IV. Consistently, $|y_{Mn}| \cong 0$ (black line). The long

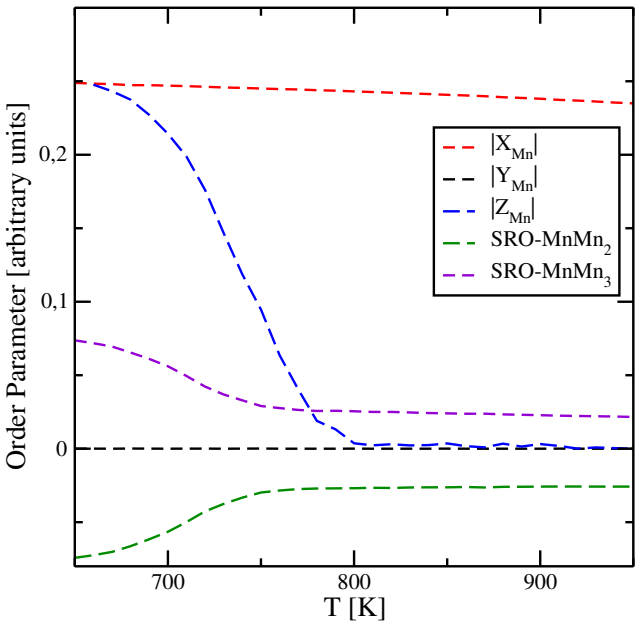

Figure 3: Thermal evolution of long and short range order parameters of manganese atoms for stoichiometric Ni_2MnAl.

range order-disorder transition can be appreciated in the variation of the parameter $|z_{Mn}|$ (blue line in Fig. 3), which vanish at $T \simeq 800K$. The variations in the order parameters are consistent with a $L2_1 \rightarrow B2$ order transition [22]. In Fig. 3, the *sro* correlations between $Mn-Mn$ pairs located as 2−nd and 3−rd neighbours are also shown. As can be seen, below the critical ordering temperature, the number of second neighbours $Mn-Mn$ pairs is zero, increasing to a non-zero value near $T_{L2_1 \rightarrow B2}$. On the other hand, the number of $Mn-Mn$ pairs as 3rd neighbours displays an opposite behaviour. This variation in the number of 2nd and 3rd neighbours $Mn-Mn$ pairs could be related with different magnetic properties. Therefore the model predicts that, by quenching at different temperatures, it is possible to obtain different ratios of $Mn-Mn$ pairs in second and third neighbours. This leads to changes in the magnetic behaviour, which will be discussed in the next subsection.

Three snapshots representing the thermal evolution of atomic ordering in Ni_2MnAl are shown in Fig. 4. The figures represent two consecutive $\{\ 1\ 0\ 0\ \}$ planes of a square section of ten lattice parameters side. The Subfig. 4a corresponds to the initial structure equilibrated at $T = 250K$: as can be seen, the ordering is not modified by thermal effects and the structure has a perfect $L2_1$ order. In Subfig. 4b the equilibrium configuration at $T = 750K$ is shown: this temperature is $\sim 50K$ below $T_{L2_1 \rightarrow B2}$. The structure has $L2_1$ long-range order, but the *sro* has been modified, with several Mn and Al atoms occupying antisite positions in sublattices III and IV, respectively; in rectangles we highlight regions where the *sro* $L2_1$ is retained. Finally, in Subfig. 4c, the equilibrium configuration obtained $\sim 50K$ above the transition temperature is displayed; $L2_1 - lro$ is broken and now Mn and Al occupy sublattices III and IV in a almost random distribution, although some *sro* correlations still persist.

3.2 Determination of magnetic interactions, critical magnetic temperatures

An estimation of the magnetic interactions to be employed in the simulations was obtained by the mean field theory, adjusting to the experimental values of the magnetic critical temperatures. Even without determining the critical behavior exactly, this method allows qualitative estimation of the magnetic interactions. The expression for critical temperature T_c (T_N Néel or T_C Curie) is given by [33, 34]

$$k_B T_c = \frac{S(S+1)}{3} \sum_p W_m^p (z_p^{\uparrow\uparrow} - z_p^{\uparrow\downarrow}) \qquad (2)$$

where k_B is the Boltzmann´s constant, S the magnetic moment, and W_m^p the magnetic exchange integral; the summation is performed over the successive (p) neighbours spheres. The variables $z_p^{\uparrow\uparrow}$ and $z_p^{\uparrow\downarrow}$ are the number of parallel and anti-parallel $p-th$ neighbours magnetic moments, respectively. For the sake of simplicity, we have considered the exchange energy as $J_m^p = W_m^p \frac{S(S+1)}{3}$.

Thus, values of J_m^2 and J_m^3 have been obtained by applying eq. 2 to available experimental results for different compositions [4, 28] and averaging over them. It should be noted that for perfect $L2_1$-fm order there are 12 3rd-neighbours with parallel moments. For the $B2$-afm configuration it has been considered that there are 4 antiparallel and 2 parallel 2nd-neighbors, since first-principles results have shown that this type of structure is energetically more stable than other possible polarization of the planes [11, 15]. Because the magnetic interaction is restricted only to manganese atoms and in both the $B2$ and $L2_1$ orders there is no first neighbour interaction between the $Mn-Mn$ pairs, J_m^1 is considered null without affecting the results.

The values obtained for the energies are

$$J_m^2 = 123.84 k_B \qquad J_m^3 = -27.86 k_B$$

that were used as parameters for MC simulations of the magnetic behaviour. These values are greater than those obtained by Simon et al [15].

In this case, the simulations were performed starting from four different initial states, namely: maximum $L2_1$ order compatible with composition; the equilibrium states 50 K below and 50 K above the order-disorder temperature; and the equilibrium state at 1400 K, which corresponds to a well defined $B2$ structure. Simultaneous evolution of the atomic configuration and magnetic state was allowed. However, since the magnetic critical temperatures of interest are well below the *lro* critical temperatures, the atomic distribution remains almost unchanged whilst the magnetic state evolves. The evolution of chemical and magnetic order parameters for $Ni_{50}Mn_{28}Al_{22}$ in a heating simulation is shown in Fig. 5. In this case, the initial structure has order $L2_1$ and it is observed that the chemical parameters only show variations relatively close to the order transition temperature (around $\sim$ 770 K) while the total magnetization vanishes at

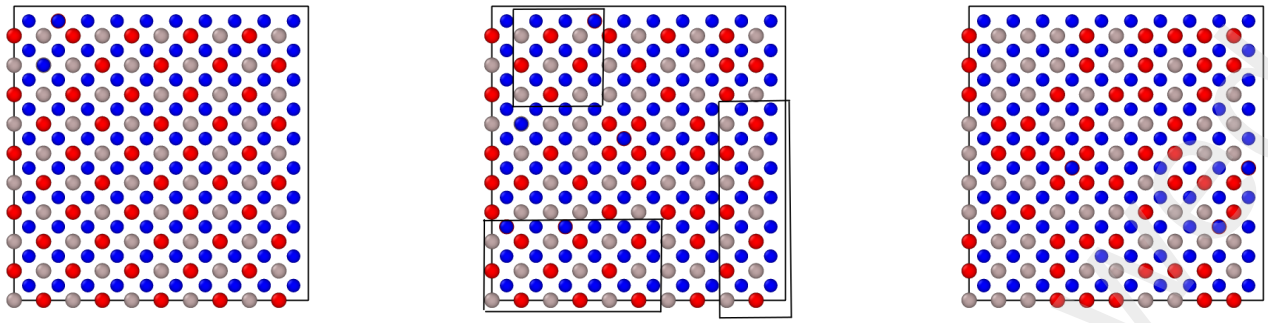

(a) Initially ordered lattice, when $L2_1$ order is perfect.

(b) Thermalized lattice at $T = 750$ K, 50 K below of phase transition. *lro* order is $L2_1$, but some aluminium and manganese atom swap positions.

(c) Thermalized lattice at $T = 850$ K, 50 K above of phase transition. There is a $B2$ order, aluminium and manganese atoms are randomly placed.

Figure 4: Snapshot at different temperatures of first layers in xy direction. Blue spheres represent nickel atoms, red spheres manganese atoms and grey spheres aluminium atoms.

a temperature of 370 K. Given the difference between the absolute values of the chemical and magnetic exchange energies, no influence of the magnetic energies on the chemical transition temperature has been detected.

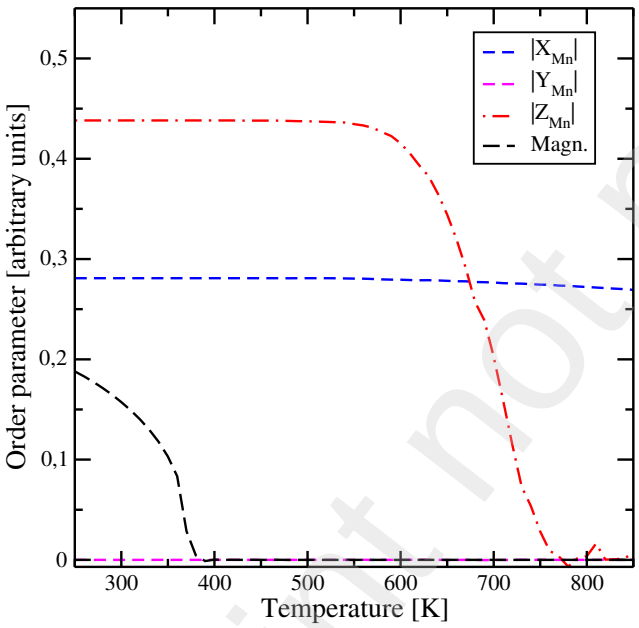

Figure 5: Heating evolution of long range order parameters of manganese atoms and total magnetization for $Ni_{50}Mn_{28}Al_{22}$.

The calculated critical magnetic temperatures for $L2_1$ and $B2$ starting configurations are shown in fig. 2 for the three studied composition lines. As expected, fm ordering for alloys with $L2_1$ configuration, and afm ordering for alloys in the $B2$ state are predicted. The overall results indicate that this model underestimates $fm - pm$ transition temperatures with respect to the experimental ones and overestimates the temperature of transitions $afm - pm$. In line $Ni_{50}Mn_xAl_{50-x}$, when $L2_1$ is present, for low manganese content the Curie temperature is low and reaches its maximum for Ni_2MnAl; when 25% manganese is exceeded, sublattice III begins to fill with manganese atoms and the Curie temperature decreases. For $B2$ order, the Néel temperature increases linearly with manganese content, unlike what was observed in the experiment [4]. In the $Ni_{75-x}Mn_{25}Al_x$ line, when manganese content remains constant, the Néel and Curie temperatures show no change with nickel and aluminium concentration, as expected. Finally, for alloys $Ni_{75-x}Mn_xAl_{50}$, the model predicts a linear increase of both critical temperatures with manganese content. Compared with another results for stoichometric Ni_2MnAl, our Monte Carlo simulations obtain a closer result than the energies obtained by ab-initio methods [15].

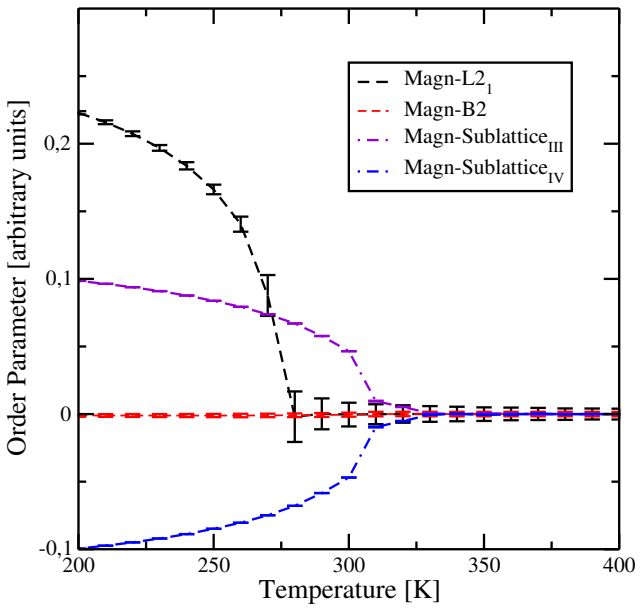

Figure 6: Evolution of magnetic order with temperature for alloy with composition $Ni_{50}Mn_{22}Al_{28}$ with different chemical ordering: quasi-perfect $L2_1$ and $B2$ order.

The thermal variation of magnetization for an alloy

$Ni_{50}Mn_{22}Al_{28}$ with different types of *lro* is displayed in Fig. 6. For an $L2_1$ configuration, a $pm-fm$ transition is observed at $T_C \sim 270K$; the net magnetization is labeled as $Magn-L2_1$ in the figure. For a $B2$ atomic state, the transition is $pm-afm$ at a Néel temperature $T_N \sim 310K$; the net and sublattice magnetizations are denoted as $Magn-B2$ and $Magn-Sublattice_i$, respectively. For $L2_1$ structure, there is a ferro- to paramagnetic transition at $T_C \sim 270$ K was found. In the other hand, for quenched $B2$ there is a para- to antiferromagnetic transition, with a Néel temperature $T_N \sim 310$ K. The effect of the difference of intensity of the second-neighbours and third-neighbours exchange energies can be seen in the fluctuations of the order parameters, added in the graphic like error bars; when the order is $B2$, the average magnetization per sublattice shows no fluctuations. On the other hand, when the order is $L2_1$, the fluctuations are greater.

4 Conclusions

In this work, a simple model based on Monte Carlo simulations for the description of atomic and magnetic ordering in ternary *bcc*-derived $Ni-Mn-Al$ alloys is implemented. The model allows simultaneous study of the configurational and magnetic degrees of freedom. A set of interchange energies in first and second neighbours for the description of atomic ordering is proposed: with this energies, a good agreement with the measured order-disorder temperatures $T_{L2_1 \rightarrow B2}$ has been obtained, for alloys along three composition lines around Ni_2MnAl. The present results indicate that the atomic ordering is strongly dominated by the attraction between Ni and Al pairs in nearest neighbours coordination. This could explain the difficulty for the development of the $L2_1$ phase from a metastable $B2$ matrix, as also found experimentally [2]: provided that the ordering in second neighbours requires transitory breaking of some first neighbours pairs, the high attraction between $Ni-Al$ could hinder the ordering in first and second neighbours.

In addition, the magnetic ordering has been simulated. Estimation of the magnetic exchange energies have been obtained by adjusting mean field expressions to experimental Curie and Néel temperatures, assuming that the only contribution is due to magnetic moments of the Mn atoms. In this way, the correct low-temperature magnetic configuration is reproduced: ferromagnetic state for $L2_1$ order, and antiferromagnetic state for the $B2$ phase. The obtained Curie or Néel critical temperatures agree qualitatively with the experimental ones in regions close to the stoichiometric composition Ni_2MnAl but they vary strongly with the amount of manganese. This result implies that the interaction is not so simple in this family of alloys and more complex methods must be employed. Moreover, it has also been studied how the magnetic transition temperature is modified when the short-range order is partially modified due to quenching. The general results show that, with a quenching of 50 K below the order transition temperature, the Curie temperature decreases around 20 K for all compositions and, when the quenching is above this transition, the Néel temperature is not affected.

Acknowledgments

This work was supported by ANPCyT (PICT 2017-4062) and CONICET (PIP 11220200102859CO). Computational facilities have been provided by the Centro de Computación de Alto Desempeño Tandil (CCADT), Facultad de Ciencias Exactas, UNCPBA. AA acknowledges postdoctoral fellowship of CONICET-Argentina.

References

[1] R. Kainuma, F. Gejima, Y. Sutou, I. Ohnuma, and K. Ishida, "Ordering, martensitic and ferromagnetic transformations in ni–al–mn heusler shape memory alloys", Materials transactions, JIM **41**, 943–949 (2000).

[2] M. Acet, E. Duman, E. F. Wassermann, L. Manosa, and A. Planes, "Coexisting ferro-and antiferromagnetism in Ni_2MnAl heusler alloys", Journal of applied physics **92**, 3867–3871 (2002).

[3] T. Mehaddene, J. Neuhaus, W. Petry, K. Hradil, P. Bourges, and A. Hiess, "Interplay of structural instability and lattice dynamics in ni2mnal", Physical Review B **78**, 104110 (2008).

[4] S. Morito, T. Kakeshita, K. Hirata, and K. Otsuka, "Magnetic and martensitic transformations in $Ni_{50}Al_xMn_{50-x}$ alloys", Acta materialia **46**, 5377–5384 (1998).

[5] P. Neibecker, M. Leitner, G. Benka, and W. Petry, "Increasing the achievable state of order in $Ni-$based heusler alloys via quenched-in vacancies", Applied Physics Letters **105**, 261904 (2014).

[6] F. Gejima, Y. Sutou, R. Kainuma, and K. Ishida, "Magnetic transformation of Ni_2AlMn heusler-type shape memory alloys", Metallurgical and Materials Transactions A **30A**, 2721–2723 (1999).

[7] T. Mehaddene, J. Neuhaus, W. Petry, K. Hradil, P. Bourges, and A. Hiess, "Interplay of structural instability and lattice dynamics in Ni_2MnAl", Physical Review B **78**, 104110 (2008).

[8] S. Morito and K. Otsuka, "Electron microscopy of new martensites with long period stacking order structures in $Ni_{50}Al_xMn_{50-x}$ alloys i. structures and morphologies.", Mat. Sci. Eng. **A208**, 47–55 (1996).

[9] A. Vovk, M. Yu, L. Malkinski, C. O'Connor, Z. Wang, E. Durant, J. Tang, and V. Golub, "Magnetic and transport properties of $NiMnAl$ thin films", Journal of applied physics **99**, 08R503 (2006).

[10] K. Ziebeck and P. Webster, "Helical magnetic order in Ni_2MnAl", Journal of Physics F: Metal Physics **5**, 1756 (1975).

[11] J. Enkovaara, A. Ayuela, J. Jalkanen, L. Nordström, and R. M. Nieminen, "First-principles calculations of spin spirals in Ni_2MnGa and Ni_2MnAl", Physical Review B **67**, 054417 (2003).

[12]T. Büsgen, J. Feydt, R. Hassdorf, S. Thienhaus, M. Moske, M. Boese, A. Zayak, and P. Entel, "Ab initio calculations of structure and lattice dynamics in $Ni-Mn-Al$ shape memory alloys", Physical Review B **70**, 014111 (2004).

[13]S. Yang, Y. Kong, Y. Du, L. Shen, and Y. Shen, "First-principles prediction of structural, mechanical and magnetic properties in Ni_2MnAl", Computational Materials Science **123**, 52–58 (2016).

[14]I. Galanakis and E. Şaşıoğlu, "Structural-induced antiferromagnetism in mn-based full heusler alloys: the case of Ni_2MnAl", Applied physics letters **98**, 102514 (2011).

[15]E. Simon, J. G. Vida, S. Khmelevskyi, and L. Szunyogh, "Magnetism of ordered and disordered Ni_2MnAl full heusler compounds", Physical Review B **92**, 054438 (2015).

[16]T. Kanomata, K. Shirakawa, and T. Kaneko, "Effect of hydrostatic pressure on the curie temperature of the heusler alloys Ni_2MnZ (Z=al, ga, in, sn and sb)", Journal of Magnetism and Magnetic Materials 65 (1987) 76-82 **65**, 76–82 (1987).

[17]N. Metropolis, A. W. Rosenbluth, M. N. Rosenbluth, A. H. Teller, and E. Teller, "Equation of state calculations by fast computing machines", The journal of chemical physics **21**, 1087–1092 (1953).

[18]A. Alés and F. Lanzini, "Atomic and magnetic ordering in bcc $Cu-Al-Mn$: computational study", Modelling and Simulation in Materials Science and Engineering **22**, 085007 (2014).

[19]M. Blume, V. J. Emery, and R. B. Griffiths, "Ising model for the λ transition and phase separation in He^3-He^4 mixtures", Physical review A **4**, 1071 (1971).

[20]F. Lanzini and R. Romero, "Thermodynamics of atomic ordering in $Cu-Zn-Al$: a monte carlo study", Computational Materials Science **96**, 20–27 (2015).

[21]E. Obradó, C. Frontera, L. Mañosa, and A. Planes, "Order-disorder transitions of $Cu-Al-Mn$ shape-memory alloys", Phys. Rev. B **58**, 14245–14255 (1998).

[22]G. Inden, "Ordering and segregation reactions in bcc binary alloys", Acta metallurgica **22**, 945–951 (1974).

[23]G. Inden, "Determination of chemical and magnetic interchange energies in bcc alloys", International Journal of Materials Research **66**, 648–653 (1975).

[24]A. Pelissetto and E. Vicari, "Critical phenomena and renormalization-group theory", Physics Reports **368**, 549–727 (2002).

[25]H. Blote, E. Luijten, and J. R. Heringa, "Ising universality in three dimensions: a monte carlo study", Journal of Physics A: Mathematical and General **28**, 6289 (1995).

[26]R. Kikuchi, "A theory of cooperative phenomena", Physical review **81**, 988 (1951).

[27]G. Inden and W. Pitsch, "Materials science and technology: a comprehensive treatment", in, Vol. 5 (VCH Weinheim, 1991) Chap. Atomic Ordering.

[28]R. Kainuma, M. Ise, K. Ishikawa, I. Ohnuma, and K. Ishida, "Phase equilibria and stability of the b2 phase in the $Ni-Mn-Al$ and $Co-Mn-Al$ systems", Journal of alloys and compounds **269**, 173–180 (1998).

[29]V. Recarte, O. Lambri, R. Pérez-Sáez, M. Nó, and J. San Juan, "Ordering temperatures in $Cu-Al-Ni$ shape memory alloys", Applied physics letters **70**, 3513–3515 (1997).

[30]R. Kainuma, X. Liu, I. Ohnuma, S. Hao, and K. Ishida, "Miscibility gap of b2 phase in $NiAl$ to Cu_3Al section of the $Cu-Al-Ni$ system", Intermetallics **13**, 655–661 (2005).

[31]J. L. Pelegrina, "A simple model to predict long-range atomic ordering temperatures in cu-based shape memory alloys", Philosophical Magazine **94**, 2705–2723 (2014).

[32]F. Lanzini, "Atomic ordering in $Cu-Al-Ni$: point approximation and monte carlo simulations", Computational Materials Science **128**, 198–206 (2017).

[33]A. Schrön, R. Rödl, and F. Bechstedt, "Energetic stability and magnetic properties of MnO in the rocksalt, wurtzite, and zinc-blende structures: influence of exchange and correlation", Physical Review B **82**, 165109 (2010).

[34]A. Ayuela, D. J. Klein, and N. H. March, "Néel temperature of antiferromagnets for phase transitions driven by spin-wave interactions", Croat. Chem. Acta **86**, 463–467 (2013).